Observations and simulations of polar cap tongue of ionization during magnetic storm on December 2006

Keisuke Hosokawa

Department of Communication Engineering and Informatics, Graduate School of Informatics and Engineering, The University of Electro-Communications, Tokyo, Japan

Also at Department of Physics, University of Oslo, Oslo, Norway

Jiuhou Lei

Department of Aerospace Engineering Sciences, University of Colorado, Boulder, Colorado, USA

Takuya Tsugawa

National Institute of Information and Communications Technology, Tokyo, Japan

Kazuo Shiokawa and Yuichi Otsuka

Solar-Terrestrial Environment Laboratory, Nagoya University, Nagoya, Aichi, Japan

Marc Hairston

University of Texas at Dallas, Dallas, USA

Correspondence

Keisuke Hosokawa
Dept. of Comm. Eng. and Informatics
University of Electro-Communications,
Tokyo 182-8585, Japan

Tel: +81 424 43 5299
Fax: +81 424 43 5293

Email: hosokawa@ice.uec.ac.jp

For submission to *Journal of Geophysical Research*

Abstract. During a magnetic storm on December 14–16, 2006, a polar cap tongue of ionization (TOI) was detected using an all-sky imager (ASI) at Resolute Bay, Canada (74.73°N, 265.07°E). We investigate the factors determining the spatial structure of the TOI by comparing the optical data with the electron density distribution derived from a Coupled Magnetosphere Ionosphere Thermosphere (CMIT) model. The CMIT model reproduces a large-scale tongue-like region of enhanced density located within the field-of-view of the ASI, which was extending continuously from a region of enhanced density in the dayside mid-latitude towards the central polar cap along the streamline of the anti-sunward convection. Even though an overall agreement is obtained between the TOI signatures in the observation and modeling, a detailed comparison demonstrates that the width of the optical TOI was much narrower than that of the large-scale density tongue in the model. This suggests that a certain process, which cannot be reproduced from the model, probably narrowed the TOI before it entered the polar cap region. Simultaneous DMSP data show that a channel of enhanced sunward convection appeared in the post-noon sector during the TOI, which is considered to be a signature of subauroral polarization stream (SAPS). Such a signature of enhanced subauroral convection is not reproduced by the model. Moreover, there was a region in which the enhanced SAPS field overlapped with the higher density plasma located equatorward of the mid-latitude trough. Hence, we propose that the SAPS, particularly the flow in its equatorward part, transported the high-density plasma in the SAPS overlap region to the noon time cusp as a narrow stream. The latitudinal width of the SAPS overlap region was almost comparable to the width of the optical plume seen in the polar cap, which confirms that the SAPS played an important role in determining the width of the TOI. This study suggests that some of the morphological characteristics of TOIs in the polar cap area can be strongly affected by flows in the duskside subauroral region. Thus, the plasma environment in the polar cap ionosphere during large magnetic storms should be described on a global perspective.

1. Introduction

When the interplanetary magnetic field (IMF) is predominantly directed southward, the rapid anti-sunward ionospheric plasma convection near the cusp inflow region, driven by the equatorial magnetopause reconnection, transports dense thermal plasma from the dayside sunlit area to the dark polar cap ionosphere. *Knudsen* [1974] first suggested that such a transport of high-density plasma results in the formation of a tongue of ionization (TOI); a TOI is a discrete channel of enhanced F region plasma that extends from the daytime sub-cusp latitudes towards the polar cap. During the transit of the TOI through the polar cap, the TOI may be broken into smaller scale density structures known as polar cap patches; a polar cap patch is a chunk of increased plasma density with spatial extent of the order of a few hundred kilometers [e.g., *Crowley*, 1996]. Numerous processes have been proposed to elcidate the detachment of daytime dense plasma from a continuous TOI in the form of discrete patches [e.g., *Milan et al.*, 2002; *Valladares et al.*, 1994; *Lockwood and Carlson*, 1992; *Anderson et al.*, 1988; *Moen et al.*, 2006], although it remains unclear which of these processes is dominant.

Several numerical models have been used to reproduce TOIs and patches in order to investigate plasma structuring process in the polar cap. *Sojka et al.* [1993] demonstrated that a TOI can be produced through enhanced dayside convection and is broken into patches if the background convection pattern has temporal variations. *Decker et al.* [1994] also modeled a TOI during a period of enhanced plasma convection and showed that the simulated density within the TOI was in reasonable agreement with f_oF_2 obtained from the digisonde at Sondrestrom. More recently, *Pryse et al.* [2009] employed electric potential patterns obtained from Super-DARN as input for the Coupled Thermosphere-Ionosphere-Plasmasphere (CTIP) model and reproduced a signature of TOI extending into the nightside across the polar cap. They obtained a good agreement between the modeled electron density within the TOI and that obtained from radiotomography. In the abovementioned modeling studies, model outputs were compared with

actual measurements and an overall agreement was obtained. However, no studies have compared model results with 2D imaging observations of TOIs in the horizontal plane. The primary obstacle to conducting such a research is a lack of 2D observations of TOI.

Foster et al. [2005] first visualized the complete 2D structure of a transpolar TOI during a severe magnetic storm on November 20, 2003, using the total electron content (TEC) data obtained from a large number of GPS receivers. It was well demonstrated that high-density plasma in the daytime mid-latitude was transported towards the nightside auroral region across the central polar cap as a discrete plume. *Foster et al.* [2005] indicated that transpolar TOIs during large magnetic storms originate from a storm enhanced density (SED; *Foster* [1993]), a longitudinally narrow stream of dense plasma formed at the equatorward edge of the duskside mid-latitude trough [*Rodger et al.*, 1992]. Later, *Foster et al.* [2007] suggested that such a plume of high-density plasma streaming poleward is carried by the low-latitude edge of enhanced convection at the subauroral latitudes; this stream is termed the subauroral polarization stream (SAPS; *Foster and Vo* [2002]). By compiling previous observational results, *Foster* [2008] claimed that the SAPS electric field plays an important role in the generation of transpolar TOIs during magnetic storms.

Recently, *Hosokawa et al.* [2009c, 2010b] introduced an optical signature of the TOI formed during a magnetic storm on December 15, 2006. They employed the 630.0 nm airglow emission obtained from an all-sky airglow imager (ASI) operating at Resolute Bay, in the northern part of Canada, to visualize the dynamic temporal evolution and small-scale spatial structure of the transpolar TOI. The optical TOI was observed as a bright airglow plume extending in the noon-midnight direction for approximately 3 h during the main phase of the storm. 1–1.5 h before the appearance of TOI, the polar cap boundary substantially expanded equatorward and an ionospheric positive storm occurred in the daytime mid-latitude region. This implied that both the "expansion of the high-latitude plasma convection" and "build up of the source

plasma in the mid-latitudes" are necessary conditions for the formation of transpolar TOIs during magnetic storms. They also demonstrated that the optical TOI changed its structure very dynamically; these changes were controlled by the temporal evolution of the enhanced SAPS electric field in the duskside subauroral region.

In this study, we extend the work of *Hosokawa et al.* [2009c, 2010b] by comparing the 2D optical observations of the TOI during the magnetic storm on December 15, 2006, with simulation results from a Coupled Magnetosphere Ionosphere Thermosphere (CMIT) model. The CMIT model [refer to *Wang et al.*, 2004; *Lei et al.*, 2008a] couples the Thermosphere-Ionosphere-Electrodynamics General Circulation Model (TIEGCM) [*Richmond et al.*, 1992] with the Lyon-Fedder-Mobarry (LFM) global magnetohydrodynamic (MHD) magnetospheric model [*Lyon et al.*, 2004], which enables us to investigate the way in which the solar-produced dense plasma in the dayside mid-latitude region can be transported towards the polar cap by the enhanced high-latitude convection electric field. Further, we focus on the differences between the TOI observed by the ASI at Resolute Bay and that reproduced by the CMIT model, and attempt to clarify the factors that determine several morphological features of a TOI. In particular, we discuss the importance of the SAPS electric field in the duskside subauroral region in characterizing the structure of TOIs.

2. Instruments and model

The ASI employed in this study was developed as a part of the Optical Mesosphere Thermosphere Imagers (OMTIs) [*Shiokawa et al.*, 1999]. The imager at Resolute Bay (74.73°N, 265.07°E; AACGM latitude 82.9°) has been operational since January 2005 [*Hosokawa et al.*, 2006]. This imager has several optical filters such as 557.7 nm, 630.0 nm, 777.4 nm, Na-line, and OH-band; this enables us to study various upper atmospheric phenomena occurring in the polar cap region, such as polar cap patches [*Hosokawa et al.*, 2006; 2009a; 2009b; 2010a], tongue of ionization

[*Hosokawa et al.*, 2009c; 2010b], polar cap aurora [*Koustov et al.*, 2008; *Jayachandran et al.*, 2009; *Hosokawa et al.*, 2010c]. In this study, all-sky airglow images at a wavelength of 630.0 nm, which are obtained every 2 min with an exposure time of 30 s, are employed. The airglow intensity at the wavelength of 630.0 nm, obtained from ground-based imagers, is known to be roughly proportional to the electron density at 200–300 km altitudes in the F region [*Barbier*, 1959; *Barbier and Glaume*, 1962]; this relationship facilitates an accurate visualization of the 2D structure of TOIs in the polar cap region.

We also employ the latest version of the CMIT model [*Wang et al.*, 2004; *Lei et al.*, 2008a], which combines the LFM global MHD magnetospheric model with the TIEGCM. The LFM magnetospheric model solves the ideal MHD equations for the magnetosphere in conservative form [*Lyon et al.*, 2004]. The TIEGCM model [*Roble et al.*, 1988; *Richmond et al.*, 1992] is a time-dependent 3D model that solves the fully coupled, nonlinear, hydrodynamic, thermodynamic, and continuity equations of the thermospheric neutral gas self-consistently with the ion continuity equations using a finite differencing scheme. This model has 29 constant-pressure levels in the vertical ranging from approximately 97 km to 500–700 km in altitude. The input parameters for TIEGCM are solar EUV and UV spectral fluxes, parameterized by the F10.7 index, auroral particle precipitation, an imposed magnetospheric electric field, and the amplitudes and phases of tides from the lower atmosphere.

These two models are coupled by exchanging parameters such as auroral precipitation and magnetospheric electric field from the LFM code and neutral wind induced currents and height-integrated conductances from the TIEGCM [*Wiltberger et al.*, 2004; *Wang et al.*, 2004]. By coupling the magnetospheric global MHD code of the LFM model with the TIEGCM, we can reproduce thermosphere ionosphere global circulation without employing empirical models of high-latitude convection electric fields and auroral precipitation. Hence, the CMIT model can self-consistently simulate a temporal evolution of the global distribution of ionospheric param-

eters under the influence of the high-latitude convection electric field imposed from the magnetosphere. This enables us to investigate the dynamical impact of the solar wind/magnetosphere on the global plasma circulation in the ionosphere during magnetic storms. The model uses a spherical geographic coordinate system in the ionosphere with a uniform latitude and longitude grid having a resolution of 5°. The spatial resolution of the model is much coarser than that of the optical data. Thus, only large-scale structures must be discussed when comparing the model results with the observations.

3. Observations and Simulations

First, we introduce the TOI detected by the ASI at Resolute Bay during the intense magnetic storm on December 14–16, 2006. This storm was primarily caused by a prolonged stable large-amplitude southward IMF within a high-speed coronal mass ejection (CME) [*Kataoka et al.*, 2009]. The provisional D_{st} index reached –146 nT at the storm peak. The optical signature of the TOI was observed for approximately 3 h (0140–0450 UT on December 15, 2006) in the early stage of the main phase of this magnetic storm. Figure 1b shows a snapshot of the 630.0 nm airglow emission at 0320 UT on December 15, 2006. The original ASI images were converted into altitude adjusted corrected geomagnetic (AACGM) coordinates [*Baker and Wing*, 1989] assuming an emission height of 250 km; these images were then mapped into MLAT/MLT coordinates. In the middle of the image, the optical signature of the TOI was observed as a continuous plume elongating in the noon-midnight direction. This elongation of the plume implies that the plume was composed of high-density plasma transported from the dayside sunlit area, which was confirmed using the ion density observations from the DMSP spacecrafts on the dayside [*Hosokawa et al.*, 2010b].

To highlight the uniqueness of the optical TOI shown in Figure 1b, we plot the 630.0 nm airglow image at 0320 UT on the previous day (December 14, 2006) in Figure 1a for comparison.

At the time this image was obtained, the upstream IMF was weakly southward around –3 nT (not shown). Hence, some signatures of polar cap patches can be identified as regions with slightly enhanced airglow intensity. It is well known that plasma within the polar cap patches is also transported from the dayside sunlit area; thus, patches potentially have some similarities to TOIs in terms of their generation process. However, if the spatial structure of the TOI is compared with that of the patches, the optical TOI is found to be almost continuous and more elongated in the noon-midnight direction while the patches are identified as individual regions of airglow enhancement. In addition, the optical intensity of the TOI is much brighter than that of the patches (indicated in the figure by the difference in the color scale). This difference may be associated with a difference in the density of the source plasma in the dayside mid-latitude. That is, the electron density in the source region is expected to be much higher during the interval of the TOI on December 15, 2006, than that on the previous day.

Figure 1d shows a map of the electron density at an altitude of around 300 km at 0320 UT on December 15, 2006, as reproduced from the CMIT model. It is demonstrated that the electron density on the daytime mid-latitude region was significantly enhanced; this enhancement is more clearly recognized by comparing this map with that obtained at 0320 UT on the previous day (Figure 1c). On December 15, 2006, the electron density at around 50° MLAT on the dayside was greater than $10^{12.0}$ m^{-3} while that on the previous day was around $10^{11.2}$ m^{-3}. This contrast suggests that an ionospheric positive storm occurred during the interval of the TOI on December 15. This is consistent with the results obtained by *Pedatella et al.* [2009], who showed that large enhancements of TEC were observed at latitudes equatorward of ≈ 70° over the Pacific Ocean region during a 4-h period from 0000 to 0400 UT on December 15. The effect of the ionospheric positive storm was found to be more prominent in the post-noon to the early evening sector than in the pre-noon sector. This region of enhanced electron density probably supplied high-density source plasma for the formation of the TOI penetrating deep into the polar cap region,

as suggested by *Hosokawa et al.* [2010b].

The notable feature in Figure 1d is the existence of a large-scale tongue-like region of enhanced electron density located in the duskside polar cap region. This structure extended continuously from the region of enhanced electron density in the dayside lower latitude towards the nightside. The electron density in the large-scale density tongue was as large as $10^{11.8}$ m^{-3}, which was almost comparable to that in the region of enhanced electron density in the dayside mid-latitude source region. This implies that the enhancement of the electron density in the large-scale tongue was not caused by local particle precipitation but by the transportation of high-density plasma from the daytime mid-latitudes to the central polar cap. In other words, this large-scale density tongue corresponds to the signature of the polar cap TOI in the CMIT model, which is compared with the optical TOI observed at Resolute Bay. It should be noted that such a large-scale electron density structure cannot be seen in the model results on the previous day shown in Figure 1c, suggesting that enhanced storm-time high-latitude convection and the occurrence of an ionospheric positive storm on December 15, 2006, were responsible for generating the TOI.

In order to determine the origin of the high-density plasma in the large-scale tongue, we plot the electron density from the CMIT model together with the contours of the electrostatic potential derived from the model in Figure 1f. A comparison of the density distribution with the background convection stream line implies that plasma in the large-scale tongue originated from the region of enhanced electron density in the post-noon to the early evening sector. In addition, on comparing the potential contours on this day with those on the previous day (Figure 1e), it is found that the high-latitude convection pattern further expanded equatorward during the interval of the TOI. Such expansion of the high-latitude electric field allowed the plasma convection to capture the high-density plasma in the lower latitudes and transported them into the polar cap region as a TOI. *Hosokawa et al.* [2010b] suggested that both the "expansion of the

high-latitude plasma convection" and "build up of the source plasma in the mid-latitudes" are necessary conditions for the formation of TOI. The CMIT model well reproduced an occurrence of these two conditions during the interval of the TOI, which supports the suggestion of *Hosokawa et al.* [2010b]

Next, we discuss the temporal evolution of the TOI signatures in the observation and model in greater detail. Figures 2a–f show the time sequence of the 630.0 nm airglow images selected at 30 min intervals from 0230 to 0500 UT on December 15, 2006. At 0230 UT (panel a), the optical TOI plume was located near the duskside edge of the field-of-view (FOV) and stayed slightly below 80° MLAT. By 0300 UT (panel b), the plume had moved slightly poleward and, at 0330 UT (panel c), reached the central part of the FOV. The image at 0330 UT is the highlight of this interval because the spatial structure of the plume was most clearly identified as a continuous channel of enhanced luminosity extending along the noon-midnight line. After 0330 UT, the plume remained almost stable for approximately 1 h although its spatial structure changed dynamically. At 0500 UT, the plume almost moved off the FOV, which is partially because the FOV shifted towards midnight with Earth's rotation. It is notable that the optical plume was far from stable; it exhibited very dynamic motion mainly in the dawn-dusk direction. For a more detail description of the temporal evolution of the optical TOI, refer *Hosokawa et al.* [2010b].

Figures 2m–r show the global distribution of the electron density obtained from the CMIT model for the corresponding optical images shown in Figures 2a–f. As mentioned above, the large-scale tongue of enhanced electron density can be identified in these images. The electron density within the large-scale tongue was larger in the earlier stage and decreased gradually after 0400 UT. The enhancement of the electron density in the source region in the daytime mid-latitudes also started decreasing after 0400 UT, probably resulting in the decay of the large-scale tongue in the polar cap. In order to directly compare the model outputs with the

optical data, we plot the modeled electron density in the vicinity of the FOV of the ASI (as indicated by the dashed circles) in Figures 2g–l with a linear color scale. It is clearly seen that the large-scale electron density tongue penetrated deep into the FOV of the ASI at Resolute Bay. More interestingly, both the optical TOI and large-scale tongue were located in the duskside part of the FOV; thus, at least the location of the TOI is well reproduced by the CMIT model. This result confirms that the plume in the optical data originated from the region of enhanced electron density in the dayside mid-latitudes.

The results from the CMIT model show an overall agreement with the TOI observed by the ASI at Resolute Bay. In particular, the model results clearly demonstrate that the high-latitude convection expanded equatorward and transported enhanced mid-latitude plasma towards the FOV of the ASI as a TOI. This again confirms the importance of the "expansion of the high-latitude plasma convection" and "build up of the source plasma in the mid-latitudes" for the formation of the TOI, as suggested by *Hosokawa et al.* [2010b]. However, on comparing the optical data in Figures 2a–f and the electron density in Figures 2g–l in further detail, some notable differences are identified in the characteristics of the optical TOI and large-scale tongue in the model. First, the width of the large-scale tongue in the CMIT model looks much broader than that of the optical TOI. Second, the optical TOI moved in the dawn-dusk direction very dynamically while the large-scale electron density tongue in the model did not show any significant motion. Later in this paper, we will focus on these differences between the observations and model results.

To obtain a better understanding of the differences, we plot the optical data and modeled electron density along the dawn to dusk cross section (i.e., 18 MLT to 06 MLT) as a function of UT in Figure 3. In the left panel, the optical data are shown in a format of keogram along the dawn to dusk cross section, as indicated by the horizontal dashed line in Figure 1b. The vertical axis is UT from 0130 to 0530 UT and the horizontal axis is MLAT from 70° on the duskside

to 80° on the dawnside across the magnetic pole, which is indicated by the vertical dashed line. In the right panels, the modeled electron density within the white rectangle shown in Figure 1d is plotted for every 10 min. Note that we again employed the linear color scale for plotting the modeled electron density. Now, the optical data in the left panel and the modeled electron density on the right can be compared directly; thus, the differences between the observations and model results are more clearly recognized.

The TOI plume first appeared at around 0140 UT near the duskside edge of the FOV. After this appearance, the TOI stayed below 80° MLAT for approximately 1 h until 0250 UT. Then, the plume suddenly started moving dawnward (i.e., poleward) and reached the zenith of Resolute Bay at 0305 UT. During this rapid excursion, the TOI moved dawnward by approximately 1000 km in about 15 min. The trajectory of the plume after this major dawnward excursion at around 0250 UT is traced by the dashed curve in the keogram to demonstrate its dynamic temporal evolution more clearly. The trace of the optical TOI is also superimposed on the electron density panels on the right to compare the motion of the optical TOI with that of the large-scale electron density tongue. After the TOI arrived at the zenith of Resolute Bay, the plume gradually shifted its sitting location toward dusk whereas the MLAT of the plume occasionally exhibited short dawnward excursions. Finally, the plume moved out of the FOV at around 0500 UT. This disappearance of the plume was associated with both the shift of the FOV with Earth's rotation and gradual duskward motion of the plume itself.

The keogram shown in the left panel of Figure 3 indicates that the width of the TOI plume along the dusk to dawn cross section varied slightly with time; however, the width was generally 3°–5° in MLAT, corresponding to a horizontal distance of 300–500 km. In contrast, the electron density within the large-scale tongue in the CMIT model was as large as 20×10^{10} m^{-3} over 10° in MLAT. Of course, it should be noted that the optical intensity is not exactly proportional to the electron density. However, the width of the optical TOI was considerably

narrower than that of the large-scale electron density tongue. In addition, the optical TOI showed a very rapid dawnward excursion at around 0250 UT while the electron density tongue does not show such a motion in the dawn to dusk direction. In reality, the electron density tongue gradually moved dawnward. However, this is probably due to the gradual change of the polar cap convection pattern, which in turn is due to the change of the IMF clock angle during this interval. In the next section, we will discuss the cause of these differences and investigate possible factors characterizing the morphological feature of TOIs.

4. Discussion and Summary

The CMIT model demonstrated that the electron density on the daytime mid-latitude region was significantly enhanced, indicating that an ionospheric positive storm occurred during the interval of the TOI. Ionospheric variations associated with this positive storm were previously investigated in detail by *Pedatella et al.* [2009], who showed that large enhancements of TEC were observed at latitudes equatorward of $\approx 70^\circ$ over the Pacific Ocean region during a 4-h period from 0000 to 0400 UT on December 15, 2006. *Lei et al.* [2008b] also used the CMIT model to demonstrate that both equatorward neutral winds and vertical drifts were increased at low to mid-latitudes during the initial stage of the ionospheric storm; both the neutral winds and vertical drifts were responsible for producing the large positive storm effect on the dayside low to mid-latitude ionosphere. Such an occurrence of ionospheric positive storm probably provided the high-density source plasma for the formation of the TOI, which is consistent with the suggestion of *Hosokawa et al.* [2010b].

Hosokawa et al. [2010b] indicated that the polar cap boundary (PCB) started expanding equatorward across the F region terminator after the IMF was directed southward at around 2230 UT on December 14. The PCB stayed at around 65° MLAT during the TOI, which is approximately 10° equatorward of its normal position. This extreme expansion of the PCB

was completed 1–1.5 h before the onset of the TOI, and the boundary returned to higher latitudes when the TOI disappeared. The CMIT model also showed that the high-latitude plasma convection expanded equatorward significantly during the interval of TOI, suggesting that the "expansion of the high-latitude convection system" was one of the necessary conditions for the formation of the transpolar TOI. As shown in Figure 1f, the greatly expanded convection gathered the high-density mid-latitude plasma in a wide local time sector from the post-noon to the early evening along the streamline of the plasma convection. This is probably the reason for the broad signature of the TOI in the model. In contrast, the width of the TOI in the optical observation was much narrower than that reproduced from the model; thus, there exists a discrepancy between the observation and modeling. In the following, we will discuss this discrepancy in greater detail.

Now, we discuss why the width of the large-scale electron density tongue seen in the model output was much broader than that of the observed optical TOI. Figure 1f shows that the large-scale density tongue was located in the duskward part of the polar cap anti-sunward convection, which indicates that plasma within the tongue was transported from the region of enhanced density extending over a wide local time sector from the post-noon to the early evening. In contrast, the optical TOI was located in a considerably limited area within the anti-sunward polar cap convection. *Hosokawa et al.* [2009c, 2010b] demonstrated by using the plasma drift measurement from the DMSP satellite that the spatial extent of the anti-sunward convection was much wider than the width of the optical plume, indicating that the TOI was already confined in the longitude before it entered the polar cap across the PCB. *Foster et al.* [2005] claimed that the SAPS field, particularly the flow in its equatorward part, plays an important role in transporting the post-noon high-density plasma to the noon time cusp as a narrow stream known as SED. We suggest that the SAPS also occurred during this interval and played an important role in narrowing the width of the optical plume.

In order to clarify the role played by the SAPS, we plot the ion drift data obtained from the DMSP F17 satellite, passing through the dayside part of the high-latitude ionosphere, in Figure 4a. The grey bars show the cross-track ion drift along the orbit of DMSP. In the dusk sector around 15–16 MLT, there existed two enhancements of the sunward convection. The one at the higher latitude corresponds to the sunward convection in the auroral zone and the other at the lower latitude is a signature of the SAPS. To compare the zonal drift obtained from the CMIT model with the DMSP data, we select the simulation grid points close to the DMSP orbit (indicated by the black line with dots in Figure 4a) and plot the modeled zonal drift indicated by the black line with dots in Figure 4b. In this panel, a positive value corresponds to the eastward drift and the DMSP cross track ion drift is also shown (grey line) for comparison. The notable feature is that the modeled zonal drift did not show any outstanding enhancements associated with the SAPS. This indicates that the CMIT model reproduced the large-scale electron density tongue without a contribution from the SAPS electric field, which is probably a reason for the difference in width between the large-scale tongue and the optical plume.

To understand how the SAPS determined the width of the optical TOI, we investigated the interaction of the mid-latitude high-density plasma with the SAPS by combining the DMSP ion drift measurement with a map of TEC. Figure 5a shows the TEC map at 0310 UT on December 15, 2006. A clear signature of the mid-latitude trough can be identified as a region of decreased TEC on the duskside. Here, the equatorward boundary of the trough is defined as an 8 TEC unit (TECU) level contour and plotted together. At this time, the trough penetrated deep into the dayside local time sector. Since a SAPS generally overlaps with the mid-latitude trough [*Basu et al.*, 2008], the SAPS also extended into the dayside and contributed to the erosion of the high-density mid-latitude plasma into the cusp as an SED. In Figure 5b, the ion drift data from DMSP F17 are superimposed on the TEC map. It can be clearly seen that the sunward ion drift was significantly enhanced within the trough, which confirms that the SAPS

actually overlapped with the trough and extended toward the earlier local time sector. Figure 5c shows the electron density distribution from the CMIT model together with the equatorward boundary of the trough identified from the TEC observations (Figure 5a). There is no apparent signature of the trough in the modeled electron density, which again suggests that the SAPS and resulting electron density depletion in the trough were not reproduced from the model.

Figure 5d shows the same data as those shown in Figure 4b; however, the equatorward boundary of the trough identified from the TEC map along the orbit of DMSP F17 is superimposed. The peak of the SAPS field was located poleward of the equatorward boundary of the trough. However, the SAPS electric field extended well equatorward of the trough. This is indicated by the existence of a region in which the strong sunward drift associated with the SAPS overlapped with the higher density region located equatorward of the trough. This is the region where the sunward SAPS convection captured the high-density plasma and transported it towards the cusp inflow region as a narrow SED stream. This is probably the reason why the observed optical TOI at the polar cap latitudes was very narrow in width. Thus, the width of the TOI observed over Resolute Bay was determined by the width of the region in which the SAPS field interacted with the plasma equatorward of the trough. It is noteworthy that the CMIT model cannot reproduce the SAPS and the mid-latitude trough. Hence, the source of the large-scale electron density tongue at the cusp inflow region was not confined in longitude; thus, the width of the electron density tongue was much broader than that of the optical TOI.

An erosion of the mid-latitude high-density plasma in the equatorward part of SAPS was already suggested by *Foster et al.* [2007]. They combined the ionospheric TEC measurements, the DMSP ion drift data, and the IMAGE EUV images and demonstrated that the equatorward edge of the SAPS electric field overlapped with the erosion plume and that the plume material was carried towards the cusp inflow region from the SAPS overlap region. Hence, the process shown in Figure 5 is not novel. However, we first propose that the width of the transpolar TOI

observed at the polar cap site can be determined by the width of the SAPS overlap region. If we look at Figure 5d in more detail, the latitudinal width of the SAPS overlap region was about 5° (≈ 500 km), which is almost comparable to the width of the optical plume observed over Resolute Bay. This value is obviously much smaller than the width of the large-scale electron density tongue reproduced from the CMIT model. This again confirms that some of the spatial characteristics of the transpolar TOI could be determined by the electric field structure in the subauroral region.

The SAPS during a magnetic storm is usually considered as a manifestation of the coupling between the low-conductance subauroral ionosphere and the ring current in the inner magnetosphere [*Foster and Burke*, 2002]. When the ring current develops in the inner magnetosphere, large pressure maxima are formed in the nightside magnetosphere, which causes Region 2 field-aligned currents (R2-FACs) flowing into the subauroral ionosphere. Intense poleward-directed electric fields are then set up to drive closure currents flowing poleward across the low-conductivity mid-latitude trough in the subauroral region. Within the region of strong plasma drifts, frictional heating enhances ionospheric recombination rates [*Schunk et al.*, 1976], resulting in reduction of the conductance. Such an ionospheric feedback process can further intensify the polarization electric fields. As long as the pressure gradients associated with the ring current exist, they drive R2-FACs, coupling the magnetosphere and ionosphere, and maintain an intense poleward electric field in the subauroral region.

In the CMIT model, the electric field structure in the high-latitude ionosphere including the subauroral region is determined by the LFM MHD simulation. MHD models can reproduce most of the observed features of Earth's magnetosphere beyond a geocentric distance of approximately 10 R_E. In the inner magnetosphere, however, their representation becomes unrealistic due to the neglect of particle transport by the energy-dependent gradient/curvature drift [*Toffoletto et al.*, 2004]. Thus, the formation/development of both the ring current and

resulting SAPS structure cannot be reproduced by a MHD model that treats plasma as a single fluid. Recently, *Ebihara et al.* [2009] employed the comprehensive ring current model (CRCM) to reproduce the storm-time SAPS observed by a mid-latitude SuperDARN radar in Hokkaido, Japan. They demonstrated that the dynamical character of the SAPS was a direct manifestation of the plasma pressure distribution in the inner magnetosphere, suggesting the importance of the spatial distribution of the ring current in the formation of the SAPS. This again implies that a non-MHD approach must be included to reproduce the evolution of the SAPS field in the subauroral ionosphere.

As mentioned above, the SAPS can be further intensified through an ionospheric feedback process working in the low-conductance mid-latitude trough. *Zheng et al.* [2008] evaluated the effects of trough conductance on the evolution of the SAPS and suggested that the low conductance at the subauroral latitude is critical to the large amplitude SAPS. Hence, in order to model the development of the SAPS accurately, we also have to simulate the further reduction of the conductance within the trough when an intense SAPS field is imposed. In summary, our comparison of the CMIT modeling of the polar cap TOI with the optical plume observed at Resolute Bay shows that the SAPS field played a critical role in characterizing the spatial structure and temporal behavior of the transpolar TOI. In order to model the structure of the polar cap TOI in greater detail, we have to include the effect of SAPS by simulating the spatial distribution of the ring current in the inner magnetosphere and ionospheric feedback process working in the low-conductance subauroral ionosphere. This suggests that the plasma environment in the polar cap ionosphere during large magnetic storms should be described on a global perspective.

Acknowledgments. This work was supported by Grants-in-Aid for Scientific Research (16403007, 19403010, 20244080 and 20740282) from the Japan Society for the Promotion of Science (JSPS).

This work was carried out by the joint research program of the Solar-Terrestrial Environment Laboratory (STEL), Nagoya University. The authors thank Y. Katoh, M. Satoh, and T. Katoh of STEL, Nagoya University, for kind support in airglow imaging observations. Special thanks are extended to staff of the Narwhal Arctic Service at Resolute Bay for kind and helpful support in operating the optical instrument. The optical observation at Resolute Bay was also supported by the NSF cooperative agreement ATM-0608577. This research was partially supported by Special Funds for Education and Research (Energy Transport Processes in Geospace, Solar-Terrestrial Environment Laboratory, Nagoya University) of the Ministry of Education, Culture, Sports, Science, and Technology of Japan. The GPS data used in this study were obtained via the ftp servers of CORS (ftp://www.ngs.noaa.gov/cors/rinex/), SOPAC (ftp://garner.ucsd.edu/pub/rinex/), and IGS (ftp://cddisa.gsfc.nasa.gov/pub/gps/data/daily/). We acknowledge the IGS, UNAVCO, SCIGN and its sponsors, the W.M. Keck Foundation, NASA, NSF, USGS, SCEC for providing GPS data. A part of this work was done while K.H. was staying at Department of Physics, University of Oslo as a guest researcher. His research at University of Oslo was supported by a grant of "Excellent Young Researcher Overseas Visit Program" from JSPS.

References

Anderson, D. N., J. Buchau, and R. A. Heelis (1988), Origin of density enhancements in the winter polar cap ionosphere, *Radio Sci., 23*, 513.

Baker, K. B., and S. Wing (1989), A new magnetic coordinate system for conjugate studies of high latitudes, *J. Geophys. Res., 94*, 9139.

Barbier, D. (1959), Recherches sur la raie 6300 de la luminescence atmosphrique nocturne, *Ann. Geophys., 15*, 179.

Barbier, D. and J. Glaume (1962), La couche ionosphrique nocturne F dans la zone intertropicale et ses relations avec l'mission de la raie 6300 du ciel nocturne, *Planet. Space Sci., 9*, 133.

Basu, Su., et al. (2008), Large magnetic storm-induced nighttime ionospheric flows at midlatitudes and their impacts on GPS-based navigation systems, *J. Geophys. Res., 113*, doi:10.1029/2008JA013076.

Crowley, G. (1996), Critical review of ionospheric patches and blobs, in *Review of Radio Science 1993-1996*, edited by W. R. Stone, p. 619, Oxford Univ. Press, New York.

Decker, D., C. Valladares, R. Sheehan, S. Basu, D. Anderson, and R. Heelis (1994), Modeling daytime F layer patches over Sondrestrom, *Radio Sci., 29*, 249.

Ebihara, Y., N. Nishitani, T. Kikuchi, T. Ogawa, K. Hosokawa, M. - C. Fok, and M. F. Thomsen (2009), Dynamical property of storm time subauroral rapid flows as a manifestation of complex structures of the plasma pressure in the inner magnetosphere, *J. Geophys. Res., 114*, doi:10.1029/2008JA013614.

Foster, J. C. (1993), Storm-time plasma transport at middle and high latitudes, *J. Geophys. Res., 98*, 1675.

Foster, J. C., and W. J. Burke (2002), SAPS: A new characterization for sub-auroral electric fields, *Eos Trans. AGU, 83*, 393.

Foster, J. C., and H. B. Vo (2002), Average characteristics and activity dependence of the subauroral polarization stream, *J. Geophys. Res., 107*, doi:10.1029/2002JA009409.

Foster, J. C., et al. (2005), Multiradar observations of the polar tongue of ionization, *J. Geophys. Res., 110*, doi:10.1029/2004JA010928.

Foster J. C., W. Rideout, B. Sandel, W. T. Forrester, and F.J. Rich (2007), On the relationship of SAPS to storm-enhanced density, *J. Atmos. Solar Terr. Phys., 69*, 303.

Hosokawa, K., K. Shiokawa, Y. Otsuka, A. Nakajima, T. Ogawa, and J. D. Kelly (2006), Estimat-

ing drift velocity of polar cap patches with all-sky airglow imager at Resolute Bay, Canada, *Geophys. Res. Lett., 33*, doi:10.1029/2006GL026916.

Hosokawa, K., K. Shiokawa, Y. Otsuka, T. Ogawa, J.-P. St-Maurice, G. J. Sofko, D. A. Andre (2009a), The relationship between polar cap patches and field-aligned irregularities as observed with an all-sky airglow imager at Resolute Bay and the PolarDARN radar at Rankin Inlet, *J. Geophys. Res., 114*, doi:10.1029/2008JA013707.

Hosokawa, K., T. Kashimoto, S. Suzuki, K. Shiokawa, Y. Otsuka and T. Ogawa (2009b), Motion of polar cap patches: A statistical study with all-sky airglow imager at Resolute Bay, Canada, *J. Geophys. Res., 114*, doi:10.1029/2008JA014020.

Hosokawa, K., T. Tsugawa, K. Shiokawa, Y. Otsuka, T. Ogawa and M. Hairston (2009c), Unusually elongated, bright airglow plume in the polar cap F region: is it tongue of ionization?, *Geophys. Res. Lett., 36*, doi:10.1029/2009GL037512.

Hosokawa, K., J.-P. St.-Maurice, G. J. Sofko, K. Shiokawa, Y. Otsuka, and T. Ogawa (2010a), Reorganization of polar cap patches through shears in the background plasma convection, *J. Geophys. Res., 115*, doi:10.1029/2009JA014599.

Hosokawa, K., T. Tsugawa, K. Shiokawa, Y. Otsuka, N. Nishitani, T. Ogawa and M. Hairston (2010b), Dynamic temporal evolution of polar cap tongue of ionization, *Journal of Geophysical Research*, submitted.

Hosokawa, K., J. I. Moen, K. Shiokawa, and Y. Otsuka (2010c), Motion of polar cap arcs, *Journal of Geophysical Research*, submitted.

Jayachandran P. T., K. Hosokawa, J. W. MacDougall, S. Mushini, R. B. Langley, and K. Shiokawa (2009), GPS Total Electron Content Variations Associated with a Polar Cap Arc, *J. Geophys. Res., 114*, doi:10.1029/2009JA014916.

Kataoka, R., T. Ebisuzaki, K. Kusano, D. Shiota, S. Inoue, T. T. Yamamoto, and M. Tokumaru (2009), Three-dimensional MHD modeling of the solar wind structures associated with 13 December 2006 coronal mass ejection, *J. Geophys. Res., 114*, doi:10.1029/2009JA014167.

Knudsen, W. C. (1974), Magnetospheric convection and the high-latitude F2 ionosphere, *J. Geophys. Res., 79*, 1046.

Koustov, A., K. Hosokawa, N. Nishitani, T. Ogawa, and K. Shiokawa (2008), Rankin Inlet PolarDARN radar observations of duskward moving Sun-aligned optical forms, *Ann. Geophys., 26*, 2711.

Lei, J., W. Wang, A. G. Burns, S. C. Solomon, A. D. Richmond, M. Wiltberger, L. P. Goncharenko, A. Coster, and B. W. Reinisch (2008a), Observations and simulations of the ionospheric and thermospheric response to the December 2006 geomagnetic storm: Initial phase, *J. Geophys. Res., 113*, doi:10.1029/2007JA012807.

Lei, J., A. G. Burns, T. Tsugawa, W. Wang, S. C. Solomon, and M. Wiltberger (2008b), Observations and simulations of quasiperiodic ionospheric oscillations and large-scale traveling ionospheric disturbances during the December 2006 geomagnetic storm, *J. Geophys. Res., 113*, doi:10.1029/2008JA013090.

Lockwood, M., and H. C. Carlson (1992), Production of polar cap electron density patches by transient magnetopause reconnection, *Geophys. Res. Lett., 19*, 1731.

Lyon, J. G., J. A. Fedder, and C. M. Mobarry (2004), The Lyon-Fedder-Mobarry (LFM) global MHD magnetospheric simulation code, *J. Atmos. Sol. Terr. Phys., 66*, 1333.

Milan, S. E., M. Lester, and T. K. Yeoman (2002), HF radar polar patch formation revisited: summer and winter variations in dayside plasma structuring, *Ann. Geophys., 20*, 487.

Moen, J., Carlson, H. C. Carlson, K. Oksavik, C. P. Nielsen, S. E. Pryse, H. R. Middleton, I. W.

McCrea, and P. Gallop (2006), EISCAT observations of plasma patches at sub-auroral cusp latitudes, *Ann. Geophys., 24*, 2363.

Pedatella, N. M., J. Lei, K. M. Larson, and J. M. Forbes (2009), Observations of the ionospheric response to the 15 December 2006 geomagnetic storm: Long-duration positive storm effect, *J. Geophys. Res., 114*, doi:10.1029/2009JA014568.

Pryse, S. E., E. L. Whittick, A. D. Aylward, H. R. Middleton, D. S. Brown, M. Lester, and J. A. Secan (2009, Modelling the tongue-of-ionisation using CTIP with SuperDARN electric potential input: verification by radiotomography, *Ann. Geophys., 27*, 1139.

Richmond, A. D., E. C. Ridley, and R. G. Roble (1992), A thermosphere/ionosphere general circulation model with coupled electrodynamics, *Geophys. Res. Lett., 19*, 601.

Roble, R. G., E. C. Ridley, A. D. Richmond, and R. E. Dickinson (1988), A coupled thermosphere/ionosphere general circulation model, *Geophys. Res. Lett., 15*, 1325.

Rodger, A. S., R. J. Moffett, and S. Quegan (1992), The role of ion drift in the formation of the ionisation troughs in the mid- and high-latitude ionosphere - a review, *J. Atmos. Terr. Phys., 54*, 1.

Schunk, R., P. Banks, and W. Raitt (1976), Effects of Electric Fields and Other Processes Upon the Nighttime High - Latitude F Layer, *J. Geophys. Res., 81*, 3271.

Shiokawa, K., Y. Katoh, M. Satoh, M. K. Ejiri, T. Ogawa, T. Nakamura, T. Tsuda, and R. H. Wiens (1999), Development of optical mesosphere thermosphere imagers (OMTI), *Earth Planets Space, 51*, 887.

Sojka, J. J., M. D. Bowline, R. W. Schunk, D. T. Decker, C. E. Valladares, R. Sheehan, D. N. Anderson, and R. A. Heelis (1993), Modeling polar cap F - region patches using time varying convection, *Geophys. Res. Lett., 20*, 1783.

Toffoletto, F. R., S. Sazykin, R.W. Spiro, R.A. Wolf, J.G. Lyon (2004), RCM meets LFM: initial results of one-way coupling, *J. Atmos. Sol. Terr. Phys., 66*, 1361.

Valladares, C., S. Basu, J. Buchau, and E. Friis-Christensen (1994), Experimental evidence for the formation and entry of patches into the polar cap, *Radio Sci., 29*, 167.

Wang, W., M. Wiltberger, A. G. Burns, S. Solomon, T. L. Killeen, N. Maruyama, and J. Lyon (2004), Initial results from the CISM coupled magnetosphere-ionosphere-thermosphere (CMIT) model: Thermosphere ionosphere responses, *J. Atmos. Sol. Terr. Phys., 66*, 1425.

Wiltberger, M., W. Wang, A. Burns, S. Solomon, J. G. Lyon, and C. C. Goodrich (2004), Initial results from the coupled magnetosphere ionosphere thermosphere model: magnetospheric and ionospheric responses, *J. Atmos. Sol. Terr. Phys., 66*, 1411.

Zheng, Y., P. C. Brandt, A. T. Y. Lui, and M.-C. Fok (2008), On ionospheric trough conductance and subauroral polarization streams: Simulation results, *J. Geophys. Res., 113*, doi:10.1029/2007JA012532.

Figure Captions

Figure 1 (a, b) 630.0 nm airglow image at 0320 UT on December 14 and December 15, 2006, respectively. The images are shown in MLAT/MLT coordinates, and the absolute airglow intensity is scaled in units of Rayleigh. Magnetic noon is at the top, and the dashed circle represents magnetic latitude of 80°. (c, d) Map of the electron density at an altitude of around 300 km reproduced from the CMIT model at 0320 UT on December 14 and 15, 2006, respectively. (e, f) Same as Figures 1c and 1d, but, in these panels, the contours of the electrostatic potential derived from the CMIT model are superimposed on the maps.

Figure 2 (a–f) Sequence of the 630.0 nm airglow images obtained at 30 min intervals from 0230 to 0500 UT on December 15, 2006. (g–l) Maps of the modeled electron density at an altitude of around 300 km in the vicinity of the FOV of the ASI, corresponding to the optical images shown in Figures 2a–f. (m–r) Global maps of the modeled electron density at an altitude of around 300 km, corresponding to the optical images shown in Figures 2a–f.

Figure 3 (left) A keogram reproduced from the 630.0 nm all-sky images along the dawn to dusk (i.e., 18 MLT to 06 MLT) cross section, as indicated by the dashed line in Figure 1b. The vertical axis is UT from 0130 to 0530 UT, and the horizontal axis is the MLAT from 70° on the duskside to 80° on the dawnside across the magnetic pole, which is indicated by the vertical dashed line. The trajectory of the plume after the major dawnward excursion at around 0250 UT is indicated by the dashed line. (right) Modeled electron density data at an altitude of around 300 km within the white rectangle shown in Figure 1d at 10 min intervals from 0140 UT to 0520 UT. The trajectory of the optical plume is indicated by the dashed line for comparison.

Figure 4 (a) Electron density and electrostatic potential contours at an altitude of around

300 km at 0310 UT on December 15, 2006, as reproduced from the CMIT model. The ion drift data obtained from the DMSP F17 satellite passing through the dayside part of the high-latitude ionosphere are superimposed on the map. Grey bars prepresent the cross-track ion drift along the orbit of DMSP. The black line with dots indicates the location of the selected simulation grid points for comparison with the DMSP ion drift data. (b) DMSP F17 cross track ion drift along the satellite track (grey) and the modeled zonal plasma drift at the simulation grid points indicated by the black line with dots in Figure 4a (black).

Figure 5 (a) TEC map at 0310 UT on December 15, 2006. The equatorward boundary of the mid-latitude trough is defined as an 8 TECU level contour and indicated by the dashed line. (b) Same as Figure 5a, but the ion drift data from DMSP F17 are superimposed. (c) Electron density distribution and electrostatic potential contours at an altitude of around 300 km, obtained from the CMIT model, together with the equatorward boundary of the mid-latitude trough identified in Figure 5a. (d) Same as Figure 4b, but the equatorward boundary of the mid-latitude trough along the orbit of DMSP F17 is indicated by the vertical dashed line.

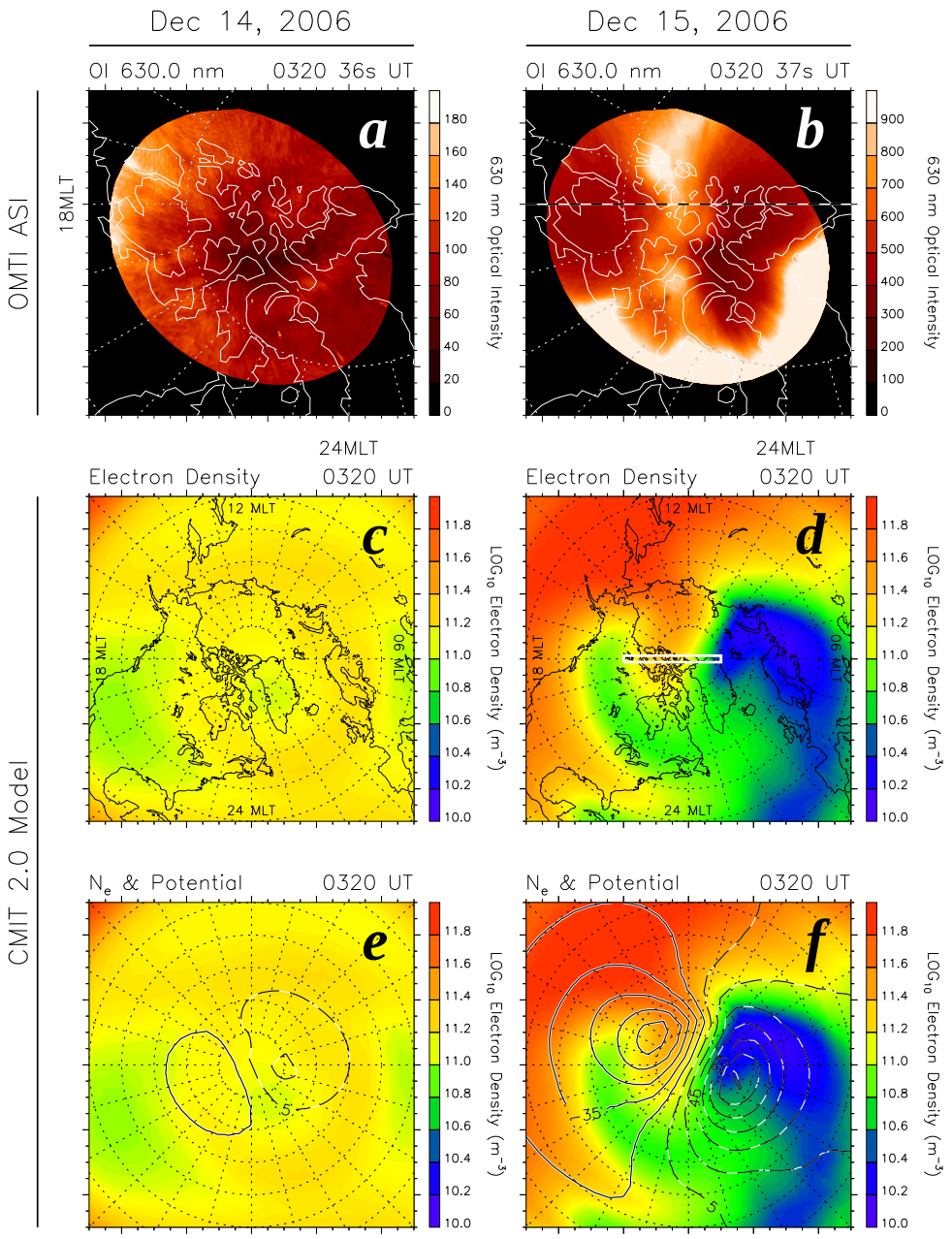
Dec 14, 2006
Dec 15, 2006
OMTI ASI
CMIT 2.0 Model
OI 630.0 nm
0320 36s UT
0320 37s UT
18MLT
630 nm Optical Intensity
24MLT
Electron Density
0320 UT
12 MLT
06 MLT
18 MLT
24 MLT
LOG10 Electron Density (m-3)
Ne & Potential
a
b
c
d
e
f

Figure 1

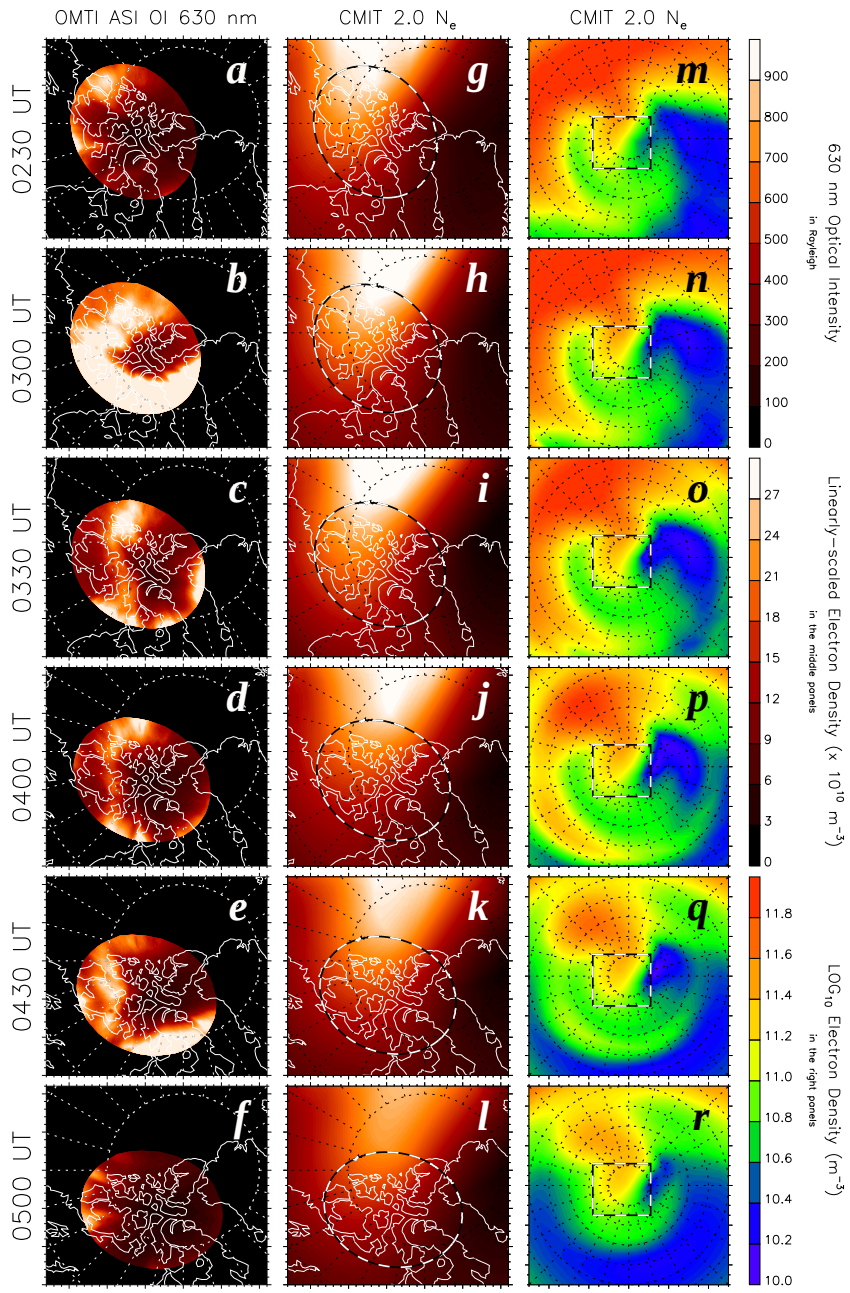
OMTI ASI OI 630 nm
CMIT 2.0 N_e
CMIT 2.0 N_e
0230 UT
0300 UT
0330 UT
0400 UT
0430 UT
0500 UT
a
b
c
d
e
f
g
h
i
j
k
l
m
n
o
p
q
r
630 nm Optical Intensity in Rayleigh
900
800
700
600
500
400
300
200
100
0
Linearly-scaled Electron Density (x 10^{10} m^{-3}) in the middle panels
27
24
21
18
15
12
9
6
3
0
LOG_{10} Electron Density (m^{-3}) in the right panels
11.8
11.6
11.4
11.2
11.0
10.8
10.6
10.4
10.2
10.0

Figure 2

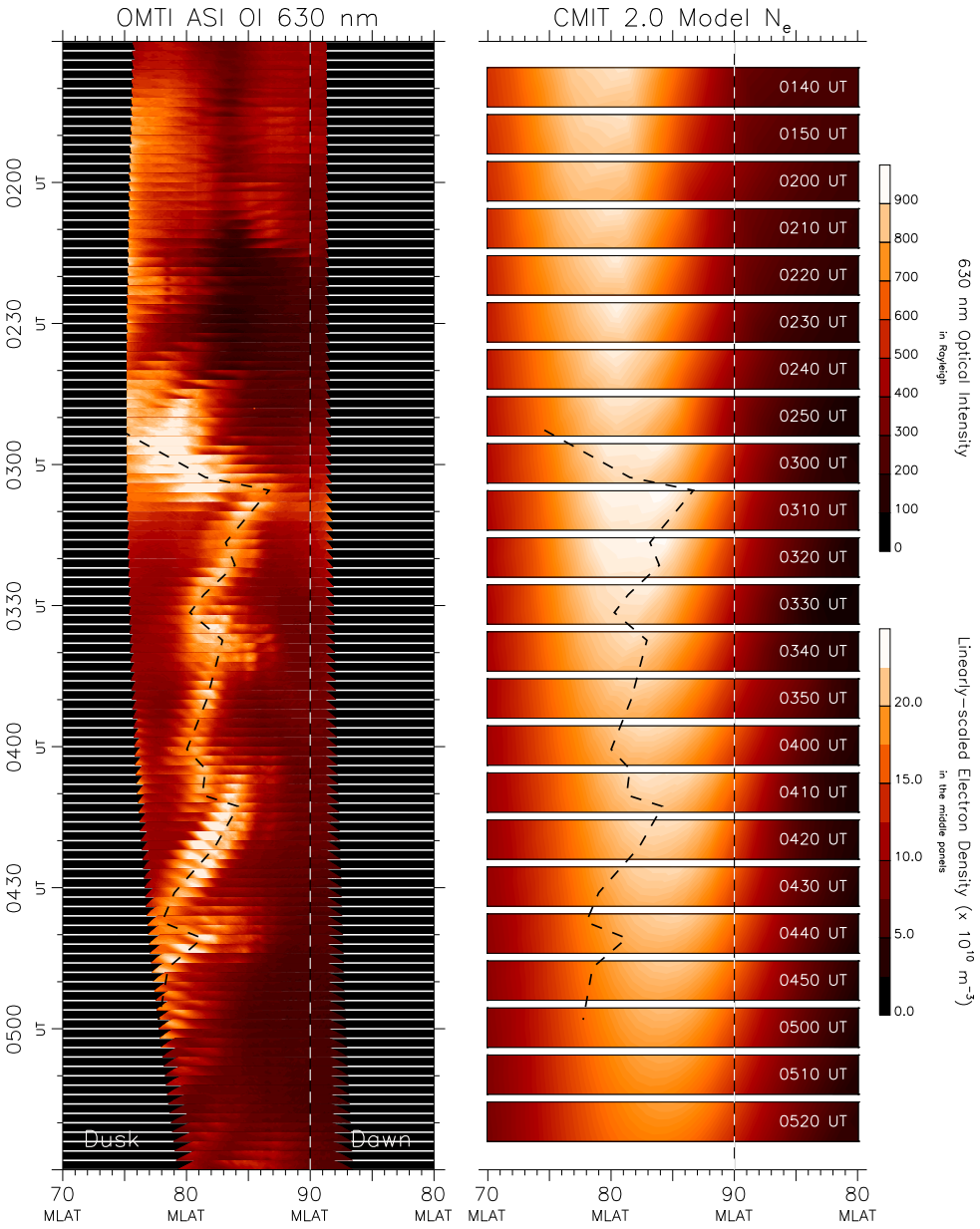
OMTI ASI OI 630 nm
CMIT 2.0 Model N_e
0200 UT
0230 UT
0300 UT
0330 UT
0400 UT
0430 UT
0500 UT
Dusk
Dawn
70 MLAT
80 MLAT
90 MLAT
80 MLAT
0140 UT
0150 UT
0200 UT
0210 UT
0220 UT
0230 UT
0240 UT
0250 UT
0300 UT
0310 UT
0320 UT
0330 UT
0340 UT
0350 UT
0400 UT
0410 UT
0420 UT
0430 UT
0440 UT
0450 UT
0500 UT
0510 UT
0520 UT
630 nm Optical Intensity in Rayleigh
900
800
700
600
500
400
300
200
100
0
Linearly-scaled Electron Density (x 10^{10} m^{-3}) in the middle panels
20.0
15.0
10.0
5.0
0.0

Figure 3

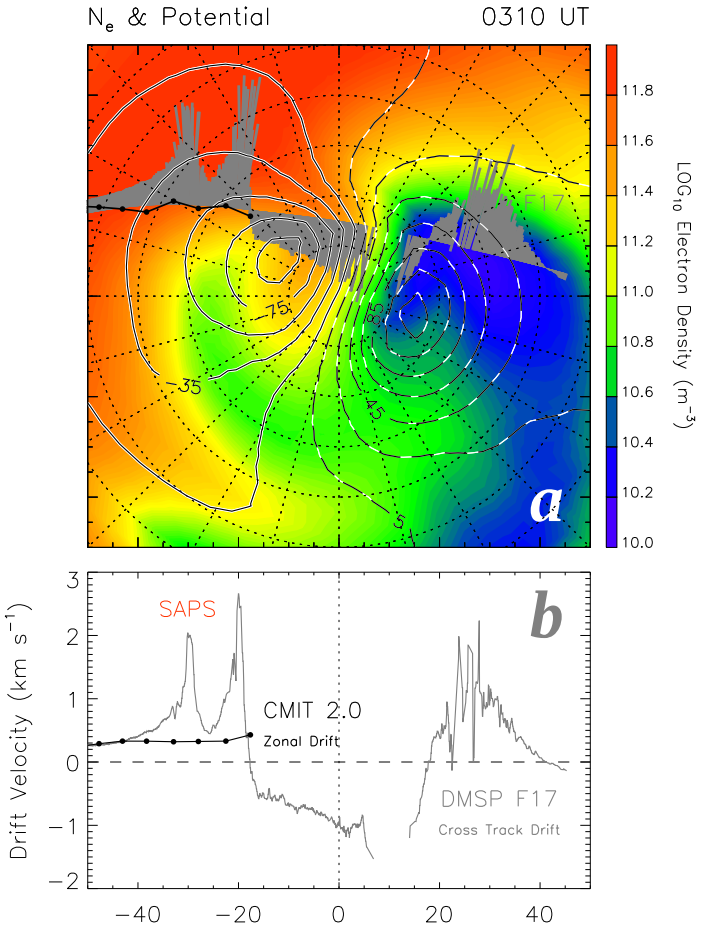
N$_e$ & Potential
0310 UT
F17
-75
-35
-5
5
45
a
11.8
11.6
11.4
11.2
11.0
10.8
10.6
10.4
10.2
10.0
LOG$_{10}$ Electron Density (m^{-3})
SAPS
b
CMIT 2.0
Zonal Drift
DMSP F17
Cross Track Drift
Drift Velocity (km s^{-1})
3
2
1
0
−1
−2
−40
−20
0
20
40

Figure 4

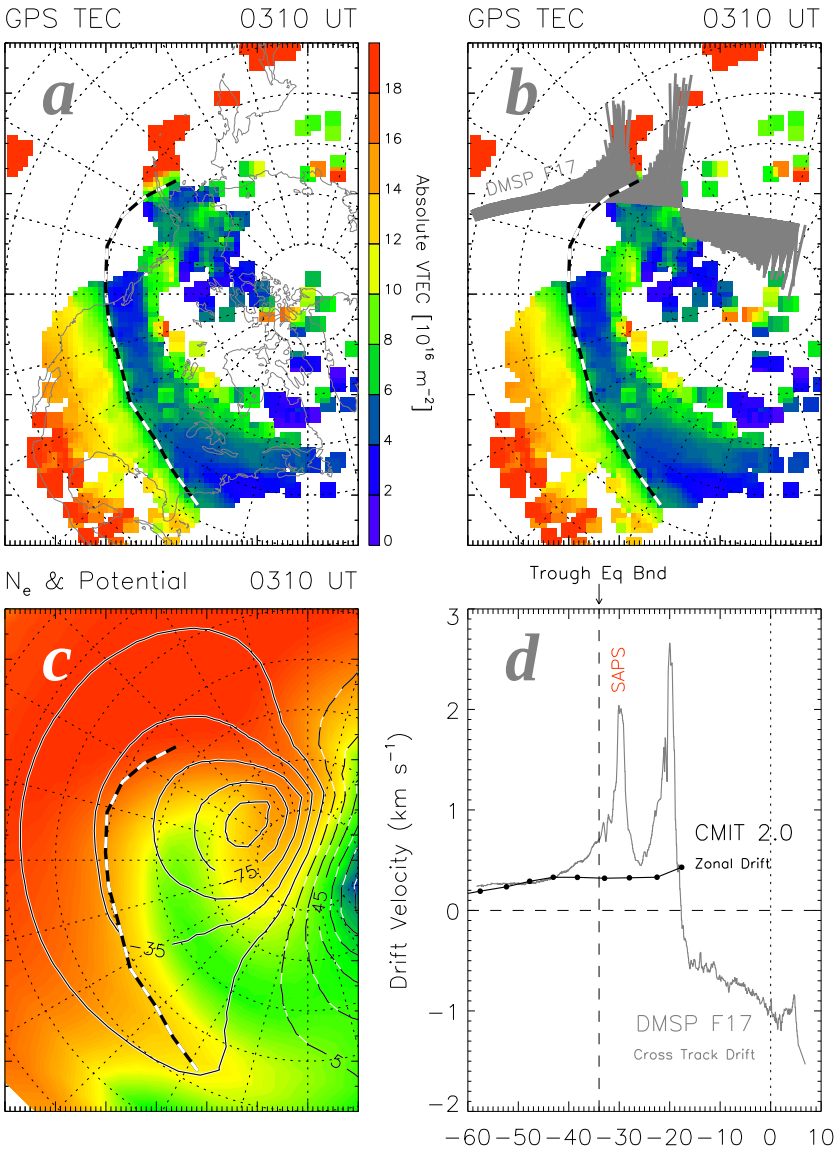
GPS TEC 0310 UT
a
18
16
14
12
10
8
6
4
2
0
Absolute VTEC [10^16 m^-2]
GPS TEC 0310 UT
b
DMSP F17
Ne & Potential 0310 UT
c
75
45
35
5
Trough Eq Bnd
d
SAPS
CMIT 2.0
Zonal Drift
DMSP F17
Cross Track Drift
Drift Velocity (km s^-1)
3
2
1
0
−1
−2
−60 −50 −40 −30 −20 −10 0 10

Figure 5